Poly(3,4ethylenedioxythiophene): poly(styrenesulfonate)/GaAs hybrid solar cells with 13% power conversion efficiency using front- and back-surface field

C.H. Lin,[2] K.W. Sun,[1,2,*] Q.M. Liu,[3] H. Shirai,[3] and C.P. Lee[2]

[1] *Department of Applied Chemistry, National Chiao Tung University, Hsinchu, Taiwan*
[2] *Department of Electronics Engineering, National Chiao Tung University, Hsinchu, Taiwan*
[3] *Graduate School of Science and Engineering, Saitama University, Saitama, Japan*
[*] *kwsun@mail.nctu.edu.tw*

Abstract: Planar hybrid solar cells based on bulk GaAs wafers with a background doping density of 10^{16} cm^{-3} and poly(3,4-ethylenedioxythiophene): poly(styrenesulfonate) (PEDOT:PSS) demonstrated an excellent power conversion efficiency of 8.99%. The efficiency of the cell was enhanced to 9.87% with a back-surface field feature using a molecular beam epitaxially grown n-type GaAs epi-layer. The efficiency and fill factor reach 11.86% and 0.8 when an additional p + GaAs epi-layer is deposited on the surface of the solar cells, which provides a front-surface field. The interface between the high- and low-doped regions in the polymer/GaAs and GaAs formed an electric field that introduced a barrier to minority carriers flow to the substrate and effectively reduced front surface carrier recombination, thereby enhancing light-generated free carrier collection efficiency and open-circuit voltage. Compared with the device without the front- and back-surface field, the fill factor and open-circuit voltage of the hybrid solar cell were improved from 0.76 to 0.8 and from 0.68 V to 0.77V, respectively. The highest efficiency reaches a record 13% when the Zonyl fluorosurfactant-treated PEDOT:PSS is used as a hole-transporting conducting layer for hybrid cells.

OCIS codes: (350.6050) Solar energy; (040.5350) Photovoltaic; (160.4890) Organic materials; (160.5470) Polymers.

References and links

1. S. Avasthi, S. Lee, Y. L. Loo, and J. C. Sturm, "Role of majority and minority carrier barriers silicon/organic hybrid heterojunction solar cells," Adv. Mater. **23**(48), 5762–5766 (2011).
2. F. Zhang, B. Sun, T. Song, X. Zhu, and S. Lee, "Air stable, efficient hybrid photovoltaic devices based on poly(3-hexylthiophene) and silicon nanostructures," Chem. Mater. **23**(8), 2084–2090 (2011).
3. X. Shen, B. Sun, D. Liu, and S. T. Lee, "Hybrid heterojunction solar cell based on organic-inorganic silicon nanowire array architecture," J. Am. Chem. Soc. **133**(48), 19408–19415 (2011).
4. S. Jeong, E. C. Garnett, S. Wang, Z. Yu, S. Fan, M. L. Brongersma, M. D. McGehee, and Y. Cui, "Hybrid silicon nanocone-polymer solar cells," Nano Lett. **12**(6), 2971–2976 (2012).
5. T. G. Chen, B. Y. Huang, E. C. Chen, P. Yu, and H. F. Meng, "Micro-textured conductive polymer/silicon heterojunction photovoltaic devices with high efficiency," Appl. Phys. Lett. **101**(3), 033301 (2012).
6. F. Zhang, D. Liu, Y. Zhang, H. Wei, T. Song, and B. Sun, "Methyl/allyl monolayer on silicon: efficient surface passivation for silicon-conjugated polymer hybrid solar cell," ACS Appl. Mater. Interfaces **5**(11), 4678–4684 (2013).
7. Q. Liu, M. Ono, Z. Tang, R. Ishikawa, K. Ueno, and H. Shirai, "Highly efficient crystalline silicon/zonyl fluorosurfactant-treated organic heterojunction solar cells," Appl. Phys. Lett. **100**(18), 183901 (2012).
8. Y. Zhu, T. Song, F. Zhang, S. T. Lee, and B. Sun, "Efficient organic-inorganic hybrid Schottky solar cell: the role of built-in potential," Appl. Phys. Lett. **102**(11), 113504 (2013).

#241273 Received 19 May 2015; revised 17 Jul 2015; accepted 21 Jul 2015; published 4 Aug 2015

9. M. Ono, Z. Tang, R. Ishikawa, T. Gotou, K. Ueno, and H. Shirai, "Efficient crystalline Si/poly(ethylene dioxythiophene):poly(styrene sulfonate): grapheme oxide composite heterojunction solar cells," Appl. Phys. Express **5**(3), 032301 (2012).
10. J. Y. Chen, C. Con, M. H. Yu, B. Cui, and K. W. Sun, "Efficiency enhancement of PEDOT:PSS/Si hybrid solar cells by using nanostructured radial junction and antireflective surface," ACS Appl. Mater. Interfaces **5**(15), 7552–7558 (2013).
11. J. Y. Chen, M. H. Yu, S. F. Chang, and K. W. Sun, "Highly efficient poly(3,4-ethylenedioxythiophene):poly(styrenesulfonate)/Si hybrid solar cells with imprinted nanopyramid structures," Appl. Phys. Lett. **103**(13), 133901 (2013).
12. B. M. Kayes, H. Nie, R. Twist, S. G. Spruytte, F. Reinhardt, I. C. Kizilyalli, and G. S. Higashi, "27.6% conversion efficiency, a new record for single-junction solar cells under 1 sun illumination," in 37th IEEE Photovoltaic Specialists Conference (PVSC, 2011), pp. 000004–000008.
13. H. Bi and R. R. Lapierre, "A GaAs nanowire/P3HT hybrid photovoltaic device," Nanotechnology **20**(46), 465205 (2009).
14. G. Mariani, R. B. Laghumavarapu, B. Tremolet de Villers, J. Shapiro, P. Senanayake, A. Lin, B. J. Schwartz, and D. L. Huffaker, "Hybrid conjugated polymer solar cells using patterned GaAs nanopillers," Appl. Phys. Lett. **97**(1), 013107 (2010).
15. J. J. Chao, S. C. Shiu, S. C. Hung, and C. F. Lin, "GaAs nanowire/poly(3,4-ethylenedioxythiophene):poly(styrenesulfonate) hybrid solar cells," Nanotechnology **21**(28), 285203 (2010).
16. J. J. Chao, S. C. Shiu, and C. F. Lin, "GaAs nanowire/poly(3,4-ethylenedioxythiophene):poly(styrenesulfonate) hybrid solar cells with incorporating electron blocking poly(3-hexylthiophene) layer," Sol. Energy Mater. Sol. Cells **105**, 40–45 (2012).
17. G. Mariani, Y. Wang, P. S. Wong, A. Lech, C. H. Hung, J. Shapiro, S. Prikhodko, M. El-Kady, R. B. Kaner, and D. L. Huffaker, "Three-dimensional core-shell hybrid solar cells via controlled in situ materials engineering," Nano Lett. **12**(7), 3581–3586 (2012).
18. J. Zhang, Y. Zhang, F. Zhang, and B. Sun, "Electrical characterization of inorganic-organic hybrid photovoltaic devices based on silicon-poly(3,4-ethylenedioxythiophene):poly(styrenesulfonate)," Appl. Phys. Lett. **102**(1), 013501 (2013).
19. E. Yablonovitch, O. D. Miller, and S. R. Kurtz, "The opto-electronic physics that broke the efficiency limit in solar cells," 38th IEEE Photovoltic Specialists Conference (PVSC), 001556–001559 (2012).
20. X. Wang, M. R. Khan, J. L. Gray, M. A. Alam, and M. S. Lundstrom, "Design of GaAs solar cells operating close to the Schockley-Queisser limit," IEEE J. Photovol. **3**(2), 737–744 (2013).
21. D. Alemu, H. Y. Wei, K. H. Ho, and C. W. Chu, "Highly conductive PEDOT:PSS electrode by simple film treatment with methanol for ITO-free polymer solar cells," Energy Environ. Sci. **5**(11), 9662–9671 (2012).
22. M. Vosgueritchian, D. J. Lipomi, and Z. Bao, "Highly conductive and transparent PEDOT:PSS films with a fluorosurfactant for stretchable and flexible transparent electrodes," Adv. Funct. Mater. **22**(2), 421–428 (2012).
23. A. Savva, E. Georgiou, G. Papazoglou, A. Z. Chrusou, K. Kapnisis, and S. A. Choulis, "Photovoltaics analysis of the effects of PEDOT:PSS-additives hole selective contacts on the efficiency and lifetime performance of inverted organic solar cells," Sol. Energy Mater. Sol. Cells **132**, 507–514 (2015).
24. F. Meillaud, A. Shah, C. Droz, E. Vallat-Sauvain, and C. Miazza, "Efficiency limits for single-junction and tandem solar cells," Sol. Energy Mater. Sol. Cells **90**(18-19), 2952–2959 (2006).
25. X. Wang, M. R. Khan, M. Lundstrom, and P. Bermel, "Performance-limiting factors for GaAs-based single nanowire photovoltaics," Opt. Express **22**(S2), A344–A358 (2014).
26. A. Kanwat and J. Jang, "Extremely stable organic photovoltaic incorporated with WO_x doped PEDOT:PSS anode buffer layer," J. Mater. Chem. C Mater. Opt. Electron. Devices **2**(5), 901–907 (2014).
27. A. M. Nardes, M. Kemerink, M. M. de Kok, E. Vinken, K. Maturova, and R. A. J. Janssen, "Conductivity, work function, and environmental stability of PEDOT:PSS thin films treated with sorbitol," Org. Electron. **9**(5), 727–734 (2008).

1. Introduction

Solar cells based on crystalline silicon are highly efficient but expensive because of the high temperatures required for their fabrication. An alternative approach that uses low-temperature processable organic semiconductors is potentially cheaper, but the resulting organic solar cells are not as efficient. Studies on the integration of organic conducting polymers with inorganic semiconductors to form hybrid organic/inorganic heterojunction solar cells provides a means of simplifying the fabrication processes and reducing costs [1–11]. The conjugated polymer, known as poly(3,4-ethylenedioxythiophene): poly(styrenesulfonate) (PEDOT:PSS), is the most widely used organic material for hybrid solar cell devices. PEDOT:PSS is transparent, conductive (1000 S/cm), and can produce a Schottky-type junction with semiconductors [4–9]. The film-forming properties of polymers can be processed at low temperature, is inexpensive to produce, and has a large area. Illuminative light is absorbed by the n-type

#241273 Received 19 May 2015; revised 17 Jul 2015; accepted 21 Jul 2015; published 4 Aug 2015

semiconductor substrate, and a hole transport layer in the PEDOT:PSS can extract holes generated in the substrate out of the device. Thus, in principle, the efficiency of the hybrid PEDOT:PSS/semiconductor solar cell is comparable with that of a conventional semiconductor p-n junction solar cell.

A number of recent studies on organic/semiconductor heterojunction solar cells were designed to augment the power conversion efficiency by spin-coating a thin PEDOT:PSS polymer layer onto silicon wafers. Techniques for improving hybrid PEDOT:PSS/Si solar cell performance have been widely studied and reported, including studies on surface sturctures [4–6,10,11], surface passivation [6], and the use of additives [7–9]. Surprisingly, relatively little work has been conducted involving hybrid heterojunction solar cells with III-V inorganic semiconductors, despite the high efficiency of III-V bulk solar cells [12].

To date, various vertically aligned nanowires have been studied in hybrid GaAs applications. A GaAs hybrid photovoltaic device with an energy conversion efficiency of 1.04% was fabricated by spin-coating poly(3-hexylthiophene) (P3HT) onto n-type GaAs nanowire arrays synthesized by molecular beam epitaxy (MBE) [13]. Solar cells based on P3HT-coated GaAs nanopillars grown on a patterned GaAs substrate using selective-area metal organic chemical vapor deposition exhibited a power conversion efficiency of 0.6% [14]. This cell efficiency was further improved to 1.44% by surface passivation of the GaAs. A heterojunction solar cell based on PEDOT:PSS and vertically aligned n-type GaAs nanowires fabricated by direct nanoetching of GaAs had a power conversion efficiency of 5.8% [15]. The efficiency of the cell was further increased to 9.2% by incorporating an electron-blocking P3HT layer [16]. More recently, a core-shell, organic-inorganic hybrid solar cell with the PEDOT shells having a controlled thickness coated onto periodic GaAs nanopillar arrays and the anionic dopants incorporated into the polymer showed a power conversion efficiency of 4.11% [17].

Using GaAs nanostructures on the surface of PEDOT:PSS/GaAs hybrid solar cells enhances the power conversion efficiency of these cells. However, the efficiency of hybrid cells with a planar structure is still relatively low, and fabricating the nanostructures increases the cost and complexity of manufacturing these cells. In this study, we investigated a hybrid solar cell composed of a PEDOT:PSS layer and a planar n-type GaAs wafer with various background doping densities. The background doping densities of the GaAs substrates were adjusted to optimize the light absorption in the depletion region and the power conversion efficiency of the planar cells. The conversion efficiency of the hybrid cells was further enhanced by incorporating a heavily-doped p+/lightly-doped n epi-layer by MBE into the surface/substarte to create a front-/back-surface field (FSF/BSF) structures.

2. Materials and methods

Two types of n-type (Si-doped) GaAs (100) wafers, denoted as samples A and B, were used to fabricate the planar PEDOT:PSS/GaAs heterojunction solar cells. The parameters of the samples are summarized in Table 1. The wafers were cleaned sequentially in an ultrasonic bath with acetone, isopropyl alcohol, and deionized water for 5 min and in HCl solution (30%) for 1 min to remove surface oxide. After cleaning, the wafers were then immediately transported to an e-beam evaporation system for Ni/Ge/Au back electrode deposition. Ohmic contact was formed by rapid thermal annealing at 420 °C for 35 sec in an N_2 atmosphere. A highly conductive polymer solution was spin-coated onto the GaAs surface by mixing a PEDOT:PSS (PH1000 from Clevios) solution with 5 wt% dimethyl sulfoxide as a secondary dopant to increase conductivity, followed by thermal annealing at 120 °C for 10 min. The best performance of the planar hybrid solar cells was achieved at a spin-coating rate of 3000 rpm for 25 sec. The wafers were soft-baked at 120 °C for 10 min to remove the residual solvent. Finally, a front anode contact was fabricated using a 60 nm-thick silver grid by thermal evaporation through a steel foil shadow mask. The performance of the solar cells was

#241273 Received 19 May 2015; revised 17 Jul 2015; accepted 21 Jul 2015; published 4 Aug 2015

analyzed using a solar simulator under air-mass 1.5 global (AM 1.5G) illumination conditions (100 mW/cm^2, 25 °C).

Samples C and D were also prepared and incorporated with a BSF structure only (sample C) and a FSF + BSF structure (sample D) in the cell. The inset in Fig. 1(a) shows the schematic of the sample structure. The device with BSF structure only was prepared using a Varian Gen II solid-source MBE machine on "epi-ready" n^+ GaAs (100) substrates with a background (Si-doping) concentration of ~10^{18} cm^{-3}. In the initial growth stage, the substrate was heated to 620 °C for 20 min under an As_2 atmosphere to desorb the native oxide. After the desorption was completed, a 3 μm-thick GaAs epi-layer with a background Si doping concentration of ~$3x10^{16}$ cm^{-3} was grown at 580 °C at 1 μm/hr growth rate with the V/III flux ratio kept slightly higher than 10. Figure 1(a) illustrates the calculated band diagram at the polymer-GaAs interface and the n–n^+ region with the BSF structures in sample C. The structure of sample D is identical to sample C except a very thin p + layer (10 nm with Be-doping to 10^{19} cm^{-3}) was grown on the top surface, which formed a FSF.

The fabrication of the completed solar cell devices (spin-coating of PEDOT:PSS, front metal contact, etc.) followed the same procedure as those for samples A and B. Figure 1 (b) shows the optical image of the device. The BSF provided a minority-carrier reflector (hole-blocking barrier) that can reduce the loss of photo-generated carriers at the back surface. The p + layer under PEDOT keeps minority carriers away from the high surface recombination area. The FSF/BSF results from band bending at the PEDOT-p^+/n–n^+ region. The reflectance (as shown in Fig. 2(a)) of the device was reduced after spin coating of the PEDOT:PSS layer because of improved index matching between the air and GaAs.

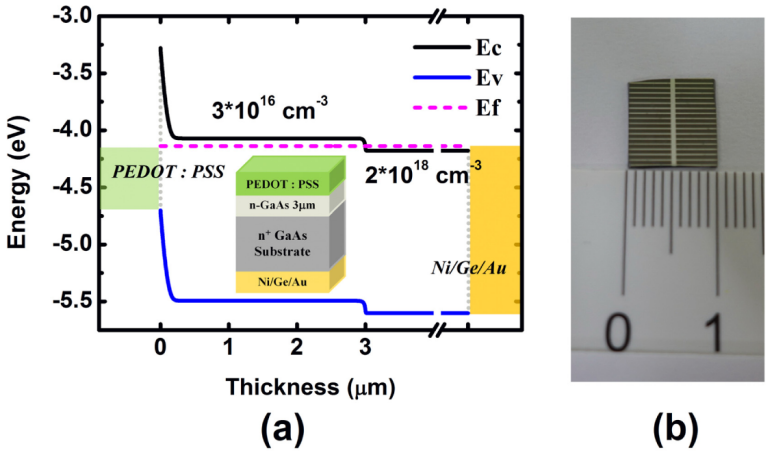

Fig. 1. (a) Calculated energy band diagram of the solar cell device with back-surface field structure. The inset shows the schematic of sample C. (b) Optical image of the device with an active area of ~1cm^2.

Table 1. Parameters of GaAs wafers used for organic/inorganic solar cell fabrication.

Substrates Parameter	Sample A	Sample B
Carrier Concentration (cm^{-3})	Si: (0.5~4)x10^{18}	Si: (3.0~5.9)x10^{16}
Carrier Mobility (cm^{2}V^{-1}s^{-1})	2240~2420	3720~3930
Wafer thickness (μm)	350	350

#241273 Received 19 May 2015; revised 17 Jul 2015; accepted 21 Jul 2015; published 4 Aug 2015

3. Results and discussion

The current density-voltage (J-V) characteristics of the devices, samples A and B, are displayed in Fig. 2(b). Sample A fabricated on a substrate with a background doping density of 10^{18} cm^{-3} yielded an open-circuit voltage (V_{oc}) of 630 mV, a short-circuit current (J_{sc}) of 10.97 mA, a fill factor (FF) of 0.7, and a power conversion efficiency (PCE) of 4.84%. With the reduction of the background doping density to $3x10^{16}$ cm^{-3}, devices B showed significant enhancement in all respects of the device performance. The overall PCE was increased significantly to approximately 9%. Figure 3 shows the measured external quantum efficiency (EQE) of samples A and B. The EQE of the device built on the substrate with a doping concentration of 10^{16} cm^{-3} was greatly enhanced throughout the entire spectrum which ranged from 300 nm to 900 nm. Assuming that a Schottky-type junction was formed between the PEDOT:PSS layer and the GaAs substrate [18], the depletion width W can be determined as $W = \frac{v_{bi}}{E_o} = \sqrt{\epsilon \epsilon_o V_{bi} / 2qN_D}$, where E_o denotes the electric field at the interface, N_D is the doping concentration, q is the electron charge, and V_{bi} is the built-in voltage. The calculated depletion width W as a function of the doping concentration in the substrate is shown in the inset of Fig. 2(b). Theoretically, increasing the W results in stronger light absorption and higher charge collection efficiency. Therefore, cells with a lower background doping densities outperform cells with higher densities. The device performance could be considered to be further enhanced using an epi-layer with an even lower background doping density. However, we found that lowering the background doping density during the growth turned the epi-layer into p-type (the inherent limitation by the MBE system), which in return, deteriorated the overall device performance.

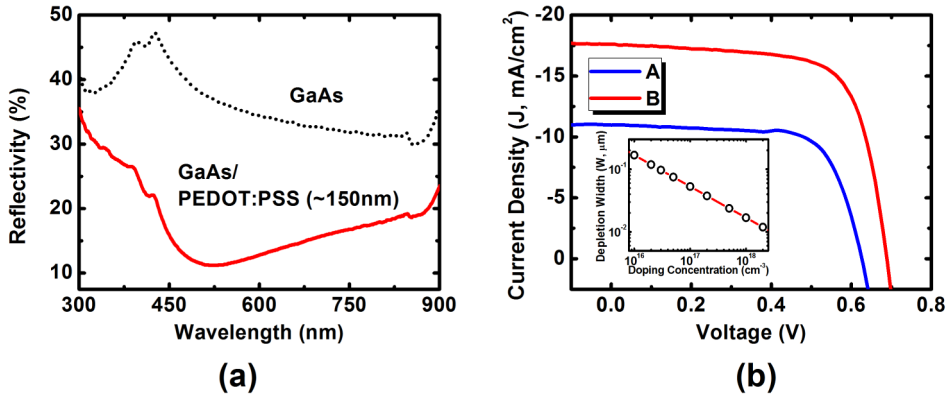

Fig. 2. (a) Reflectance spectra of GaAs with and without PEDOT:PSS layer. (b) Current density-voltage characteristics of devices A and B with different substrate background doping densities. The calculated depletion width W as a function of the doping concentration in the substrate is shown in the inset.

The J-V characteristics of the devices B, C, and D (without FSF/BSF, with BSF-only, and with FSF/BSF) are shown in Fig. 4. The V_{oc}, J_{sc}, and PCE of the solar cells incorporated with FSF/BSF structures improved significantly from 0.68 V to 0.77V, 17.52 mA/cm^2 to 19.31 mA/cm^2, and from 9% to 11.86%, respectively, compared with device B. One may argue that the observed photovoltaic effect in device D could possibly result from a GaAs homojunction between the P^+-GaAs and n-GaAs. Figure 5 shows the I-V characteristic of the device made by directly depositing a metal contact on sample D (without PEDOT:PSS coating) under dark and light (AM1.5) conditions. A turn-on voltage of ~0.35 V does not agree with the value of a typical GaAs PN homojunction [19,20]. Under AM1.5, the photovoltaic performance of this

#241273 Received 19 May 2015; revised 17 Jul 2015; accepted 21 Jul 2015; published 4 Aug 2015

device is very poor (see Fig. 5(b)). The open circuit voltage, short circuit current, fill factor, and efficiency are 0.18 V, 0.113 mA, 0.3, and 0.025%, respectively. It indicates that the photovoltaic effect of device D, shown in Fig. 4, is indeed mostly originate from a heterojunction between the PEDOT:PSS and GaAs.

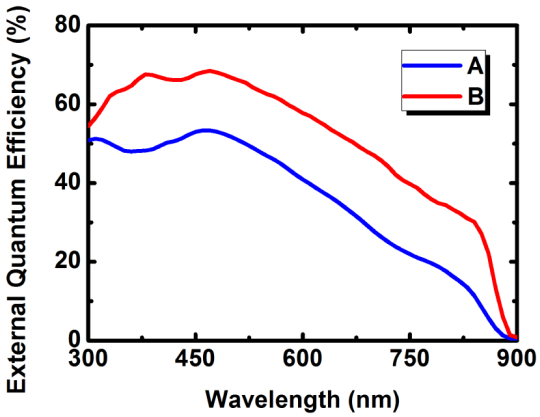

Fig. 3. External quantum efficiency (EQE) spectra of the devices A and B.

The J-V characteristics of the devices B, C, and D (without FSF/BSF, with BSF-only, and with FSF/BSF) are shown in Fig. 4. The V_{oc}, J_{sc}, and PCE of the solar cells incorporated with FSF/BSF structures improved significantly from 0.68 V to 0.77V, 17.52 mA/cm^2 to 19.31 mA/cm^2, and from 9% to 11.86%, respectively, compared with device B. One may argue that the observed photovoltaic effect in device D could possibly result from a GaAs homojunction between the P^+-GaAs and n-GaAs. Figure 5 shows the I-V characteristic of the device made by directly depositing a metal contact on sample D (without PEDOT:PSS coating) under dark and light (AM1.5) conditions. A turn-on voltage of ~0.35 V does not agree with the value of a typical GaAs PN homojunction [19,20]. Under AM1.5, the photovoltaic performance of this device is very poor (see Fig. 5(b)). The open circuit voltage, short circuit current, fill factor, and efficiency are 0.18 V, 0.113 mA, 0.3, and 0.025%, respectively. It indicates that the photovoltaic effect of device D, shown in Fig. 4, is indeed mostly originate from a heterojunction between the PEDOT:PSS and GaAs.

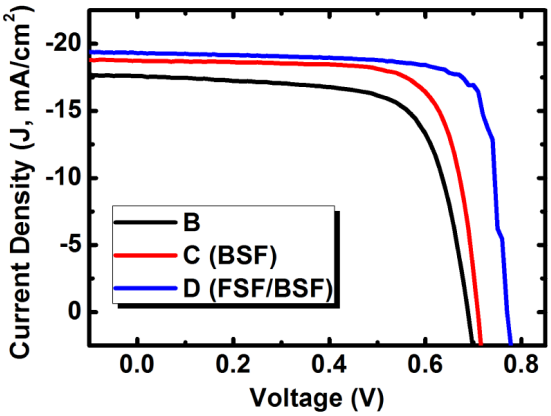

Fig. 4. Current density – voltage (J-V) characteristics of devices B (without FSF/BSF), C (BSF-only) and D (FSF/BSF).

#241273 Received 19 May 2015; revised 17 Jul 2015; accepted 21 Jul 2015; published 4 Aug 2015

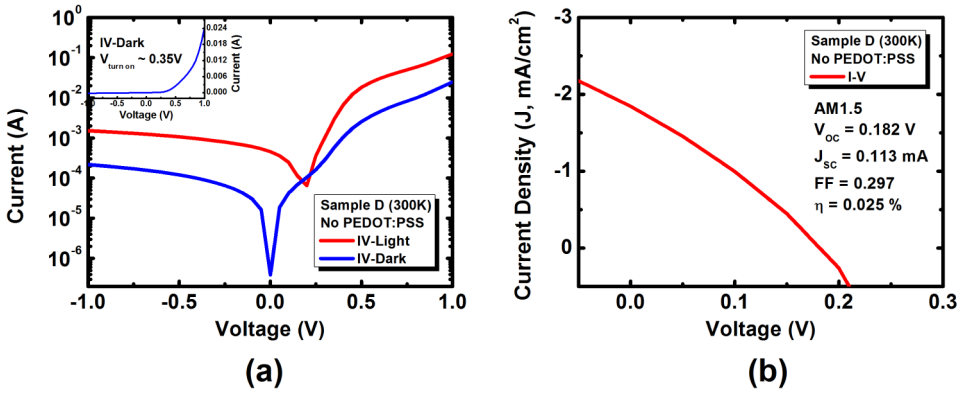

Fig. 5. (a) I-V characteristic (log scale) of the device made by directly depositing a metal contact on sample D under dark and light (AM1.5) conditions. The inset shows the I-V curve of dark condition in linear scale. (b) The photovoltaic characteristics of the device in (a).

Figure 6(a) shows the measured external quantum efficiency (EQE) and reflectance spectra of the hybrid solar cells B, C and D. The EQE of the device without FSF/BSF reached a maximum of 70% at approximately 470 nm and rapidly decreased to 900 nm. The solar cell devices C and D clearly outperformed device B in EQE at longer wavelengths (from 600 nm to 900 nm) because the carriers generated by photons with lower energy were found deep in the substrate and closer to the minority carrier blocking barrier at the n-n + interface. The carriers generated or diffused near the n-n + interface were allowed to quickly separate with minimal recombination. Therefore, the improvement in V_{oc}, and in carrier collection efficiency can be attributed to energy barrier provided by the BSF and the minority carrier reflector architecture.

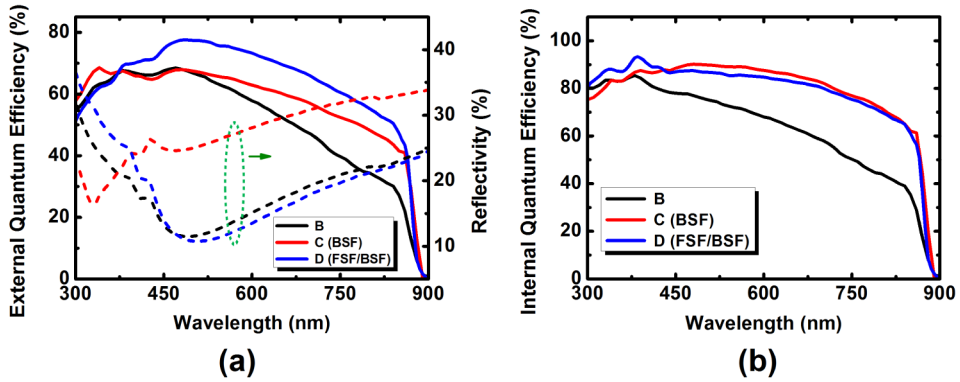

Fig. 6. (a) External quantum efficiency (EQE) and reflectance spectra (b) IQE spectra of the hybrid solar cells B, C and D.

Figure 6(a) shows that the device with BSF-only structure results in slightly lower EQE than the one without FSF/BSF for wavelength ranging from 380 nm to 480 nm. Nevertheless, at an even shorter wavelength (< 400 nm), devices C again outperformed device B. This discrepancy was simply due to the difference in the reflectance (or absorption) properties between samples B and C. The carriers generated near the surface by photons with high energy were at a distance from the n-n + (BSF) region. Therefore, the BSF had limited effect on those carriers. By contrast, the surface reflection was further reduced when the GaAs was coated with a thin PEDOT:PSS layer having a medium refractive index of approximately 1.48. However, because of the difference in the actual thickness of the organic layers deposited on samples B, C, and D (under the same spin-coating procedure) were slightly

#241273 Received 19 May 2015; revised 17 Jul 2015; accepted 21 Jul 2015; published 4 Aug 2015

different. The thicknesses of the polymer layers were 50 nm, 62 nm, and 55 nm for devices B, C, and D respectively. Parallel comparison of the reflectance spectra with the EQE (Fig. 6(a)) showed that the behavior of the EQE from 300 nm and 600 nm was clearly and strongly affected by the difference in reflectivity.

The EQE of sample D was generally improved throughout the entire spectrum compared to samples C and B (Fig. 6(a)) expect in UV (300 nm to 380 nm). The less improvement of EQE in UV for device D is also due to the effect of surface reflectance. In order to examine the effects of the FSF/BSF on the device performance and to exclude the influence of the thickness uncertainty in organic film, we have calculated the internal quantum efficiency (IQE) of devices B, C, and D using IQE = EQE/(1-R). The calculated IQE spectra (Fig. 6(b)) show enhancement from FSF/BSF but exclude any reflective effect associated with the surface. The results from the IQE spectra clearly indicate that the improvement in the EQE and V_{oc} of both sample C and D at wavelengths below ~400 nm benefits from the BSF. On the other hand, at wavelengths between 300 nm to 450 nm, the IQE and V_{oc} of device D are further improved by the FSF. The gain of IQE in UV for device D is attributed to the reduced recombination and enhanced carrier extraction caused by the FSF near the surface. The small difference in the IQE of samples C and D between 450 nm to 900 nm (Fig. 6(b)) is due to variation in the background doping of the wafers.

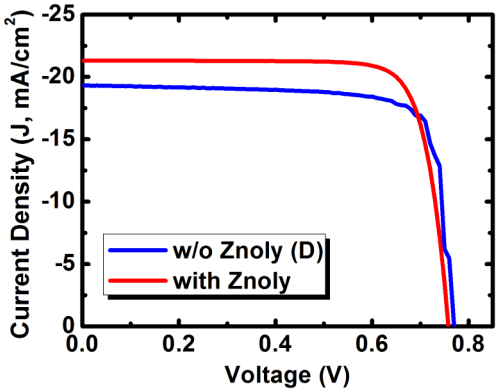

Fig. 7. Current density – voltage (J-V) characteristics of device D (FSF/BSF) with MeOH- and Zonyl-treated PEDOT:PSS layer. J-V curve of the device without treatment is also displayed in parallel for comparison.

Performance of the devices D was further enhanced with the PCE reached a record of 13% by treating the PEDOT:PSS with MeOH and Zonyl fluorosurfactant [7,21,22]. The PEDOT:PSS solution contained 5wt% DMSO, 45wt% PH1000, 50wt% MeOH and additional 0.1wt% Zonyl. Figure 7 shows the I-V curve of the device with J_{sc} improved from 19.31 mA to 21.3 mA while maintaining V_{oc} and FF. The increase in J_{sc} is due to the enhanced hole mobility by the addition of MeOH and Zonly [7]. This additive not only can enhance the electronic properties (electrical conductivity, for example) of PEDOT:PSS but also lead to improved wettability of the active layer surface. Detail studies of those additives can be found in Ref [23]. Performance of the current device outperforms best OPV (~12%) and is on a par with the best PEDOT:PSS/Si hybrid solar cells (~13%). Note that the best J_{sc} of the device (~21 mA) demonstrated in this work is still much lower than the theoretical limit of GaAs single-junction solar cell (~31 mA) [24]. The limiting factors are the short carrier lifetimes and diffusion lengths in bulk materials. However, by using thin GaAs cell structures with hundreds of nm thickness (e.g. wafer bonding, substrate lift-off) and the combination of textured surfaces and reflective back surfaces (Al mirror, for example), one can potentially achieve efficiencies over 30% under one sun AM1.5G solar spectrum [24,25]. Regarding to the stability of PEDOT:PSS thin film, although the material is extremely hygroscopic and

#241273 Received 19 May 2015; revised 17 Jul 2015; accepted 21 Jul 2015; published 4 Aug 2015

post-deposition treatments in air by thermal annealing are generally unstable due to the fast water uptake. However, long term stability of PEDOT:PSS thin film can be readily achieved by, for example, doping with WO_x nanocrystals [26] or by adding different concentrations of sorbitol [27]. In the end, we summarize the performances of devices made in this study in Table 2.

Table 2. Performances of PEDOT:PSS/GaAs hybrid solar cell.

Sample	J_{SC} (mA/cm^2)	V_{OC} (V)	FF	Efficiency (%)
A	10.97	0.63	0.70	4.84
B	17.52	0.68	0.76	8.99
C	18.76	0.71	0.74	9.87
D	19.31	0.77	0.80	11.86
D (Znoly)	21.30	0.76	0.80	13.0

4. Conclusion

In conclusion, we investigated the effects of background doping concentrations of the substrates on the performance of the PEDOT:PSS/GaAs planar hybrid solar cells and the enhancement in PCE with integrated FSF/BSF structures. The lower background doping in the substrate provided a wider depletion area which increased light absorption and enhanced charge separation. The carrier collection efficiency of the solar cells was further enhanced by the FSF/BSF structures because of the blocking of the minority carrier and reduced surface recombination and the improved hole mobility in PEDOT:PSS. The V_{oc}, J_{sc}, fill factor, and PCE of the hybrid solar cells integrated with FSF/BSF structures were significantly enhanced compared with the devices without FSF/BSF. Because of the short carrier lifetime in GaAs, one would expect that the J_{sc}, FF, and V_{oc} of the devices with FSF/BSF can be significantly improved by reducing the thickness of the active layer, texture surfaces and optimizing the background doping density of the GaAs epi-layer.

Acknowledgments

This work was supported by the Ministry of Science and Technology of the Republic of China (Contract no. NSC 102-2112-M-009-011-MY3) and the Approaching Top University Program of the Ministry of Education of the Republic of China.

#241273 Received 19 May 2015; revised 17 Jul 2015; accepted 21 Jul 2015; published 4 Aug 2015